Anal. Method Environ. Chem. J. 3 (2) (2020) 74-81

AMECJ

Research Article, Issue 2
Analytical Methods in Environmental Chemistry Journal
Journal home page: www.amecj.com/ir

One-step synthesis of zinc-encapsulated MCM-41 as H_2S adsorbent and optimization of adsorption parameters

Nastaran Hazrati [a], Ali Akbar Miran Beigi [*,b], Majid Abdouss [a] and Amir Vahid [b]

[a] *Department of Chemistry, Amirkabir University of Technology, Tehran, Iran.*
[b] *Oil Refining Research Division, Research Institute of Petroleum Industry, Tehran, Iran.*

ARTICLE INFO:

Received 20 Feb 2020
Revised form 19 Apr 2020
Accepted 10 May 2020
Available online 29 Jun 2020

Keywords:
Zinc encapsulated MCM-41,
H_2S gas,
Adsorption,
Extraction,
UOP163 method

ABSTRACT

The nano-sized structure of well-ordered Zn@MCM-41 adsorbent was synthesized through a direct hydrothermal method using CTAB as a structure-directing agent in an ammonia aqueous solution with different amounts of zinc acetylacetonate which were inserted into the structure-directing agent's loop during the synthesis. The XRD, HRTEM, and N_2 adsorption-desorption isotherms were used to characterize the prepared ZnO functionalized mesoporous silica samples. As a result, the presence of ZnO in highly-ordered MCM-41's pore was proved as well as maintenance of the ordered meso-structure of MCM-41. The materials were possessed with a high specific surface area (1114-509 m^2 g^{-1}) and a large pore diameter (4.03-3.27 nm). Based on the obtained results from the adsorption of H_2S gas in a lab-made setup, the Znx@MCM-41 showed the superior ability to increase of ZnO amount up to 7 hours as a breakthrough point. A two factor (zinc percent and temperature) experimental design with three levels was accomplished to optimize the adsorption parameters. The influence of parameters and the interactions on the adsorption of H_2S were studied and optimized. Also, the H_2S breakpoint curves carried on by UOP163 method.

1. Introduction

In recent years, the preparation and application of nano-sized materials due to their large surface areas have received by increasing attention in various areas of research [1-5]. Nano-ordered MCM-41 is a mesoporous well-ordered structure with a narrow pore size between 1.5 and 10 nm and a high surface area up to 1500 m^2 g^{1-} [6-8]. MCM-41 is a net silica network possessing, the slight acidity and low-capacity ion-exchange [9] which has great uses in many fields such as catalysis [10, 11], separation [12], medicine [13], and hydrogen sulfide removal [5, 14-16]. Giving in hand that pure siliceous MCM-41 may have limited applications [17], setting chemical-bonded functional groups in the MCM-41 channels [18], make it as a well-heterogeneous reusable catalyst in most of the reactions. Therefore, much of the research has been done to prepare the active substance through the modification of the silicate framework of MCM-41 by inorganic elements or organic functional groups [19]. Different methods for inorganic functionalization of mesoporous silica have been considered like the addition of inorganic compounds to the sol-gel mixture [20], template ion-exchange

* Corresponding Author: Ali Akbar Miran Beigi
Email: miranbeigiaa@ripi.ir
https://doi.org/10.24200/amecj.v3.i02.104

method [21], impregnation of calcined silica [22, 23, 5], chemical vapor decomposition [24, 19], and using metal-containing templates [25]. Desulfurization process, as one of the main applications of metal-containing mesoporous silica, is the most interesting area of research for lowering the sulfur-containing material, especially in oil industry [16, 26]. Hydrogen sulfide (H_2S) is a naturally occurring toxic and malodorous gas contained in most of the world's crude oils. Not only it may harm product value, but also it compromises environmental and safety compliance, such as infrastructure damages from corrosion attack, producing odors, and more. The environmental impacts on the sulfur content have forced on refiners to produce the clean petrochemical products. That is why managing hydrogen sulfide content is one of the every-stage challenges hydrocarbon processing, refining, and transportation [27]. In different industries, the H_2S can be removed using a variety of the physical-chemical and the biological methods. These methods include the Claus process, the chemical oxidants, the caustic scrubbers, H_2S scavengers, the liquid amine absorption, the liquid-phase oxidation, the physical solvents, as membrane-based processes, biological procedure, and the adsorptive methods [27, 19]. After the studies of Westmoreland et al., the H_2S adsorbents were applied based on zinc, copper, iron, and calcium oxides as proper elements due to their thermal stabilities as well as sulfur removal efficiencies. However, based on thermodynamic point of view, it can be indicated that the ZnO is an outstanding adsorbent with high efficiency for sulfur removal because of the high equilibrium constant. Furthermore, the ZnO is considered as a profitable stable sorbent as compared to many other metal oxides [28]. Herein, we described the characterization and the synthesis of zinc-incorporated MCM-41 through in-situ insertion of zinc complexes into the hydrophobic loops of micelles of structure directing agent. Therefore, the H_2S was efficiently adsorbed on zinc-incorporated MCM-41.

2. Experimental

2.1. Reagents and Materials

Tetraethylorthosilicate (TEOS), cetyltrimethylammonium bromide (CTAB), sodium acetate, zinc acetylacetonate ($Zn(acac)_2$), ethanol, ammonia and acetone were purchased from Merck company and used as received without any further purification. All of reagents were purchased from Merck. Germany.

2.2. Preparation of Zinc-incorporated MCM-41

A mixture of TEOS, cetyltrimethylammonium bromide CTAB, sodium acetate, ethanol, ammonia, deionized water (DW) and $Zn(acac)_2$ with the following molar composition (1+5x), 0.3, 1.5, 1, 14, 20 and x was used for the synthesis of Zinc-incorporated MCM-41. To start the synthesis, the proper amount of CTAB and sodium acetate was dissolved in water. Next, the dissolved $Zn(acac)_2$ (in ethanol and ammonia) were added to the solution. While stirring, TEOS was added, and after 70 minutes of stirring in 35°C, the suspension was poured into the stainless steel autoclave and heated at 70 °C for 24 hours. The obtained precipitate was filtered and then, washed with the applicable amount of acetone and DW, respectively. The prepared samples were calcined in 550 °C for 5 hours (1 °C min^{-1}). The prepared sample of Znx@MCM, where x indicates the percent of zinc (%) in the product were characterized by angle X-ray diffraction, nitrogen physisorption and high-resolution transmission electron microscopy. Also, the ability of Znx@MCM for H_2S adsorption was investigated.

2.3. Characterization

X-ray diffraction patterns were recorded on a Philips 1840 diffractometer with a Nickel-filtered Cu Kα anode (1.5418˚ A). Textural analyses were carried out on a Micromeritics Tristar 3020 system by determining the nitrogen adsorption–desorption isotherms at -196 °C. Before the analysis, the samples were degassed in vacuum for 5 hours at 300 °C until a stable vacuum of 0.1 Pa was reached. The Brunauer–Emmett–Teller (BET)

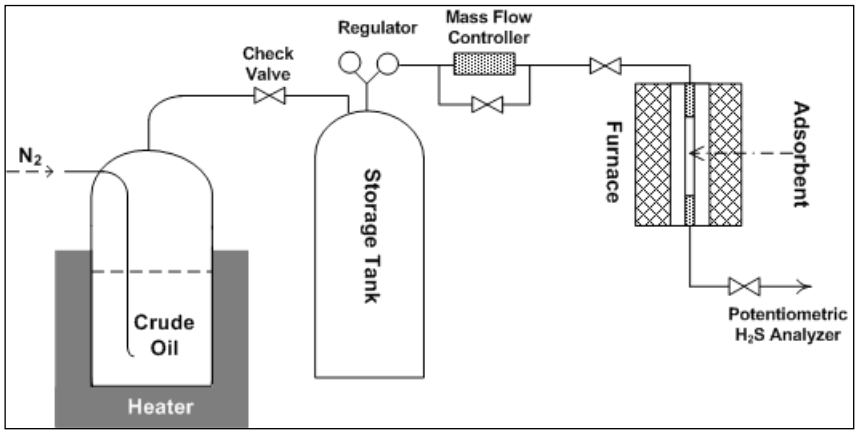

Fig. 1. Schematic plan of experimental set-up

specific surface area and the total pore volume was calculated for all of the samples. The mean pore diameter was determined by applying the Barrett–Joyner–Halenda (BJH) model. The wall thickness was calculated as the difference between the lattice parameter (a0) and the pore diameter. Transmission electron microscopy (TEM) images were obtained by a 200 kV Schottky field emitter high resolution transmission electron microscopy equipped with TEM.

2.4. Desulfurization process

H_2S of Naftshahr crude oil of Iran was extracted by cold stripping and collecting in a cylinder. The concentration of hydrogen sulfide in LPG was 5000 ppm (mg L^{-1}) as the final criterion for the H_2S breakthrough. Adsorption measurements for H_2S were accomplished using a lab-made setup (Fig. 1). The reactor effluent stream was analyzed by UOP163 method which gave the H_2S breakpoint curves.

3. Results and Discussion

3.1. X-ray diffraction

All of the samples were characterized by X-ray diffraction (XRD) to get structural confirmations about the porosity and structure of the materials. XRD patterns of the synthesized samples are given in Figure 2. The low angle patterns of prepared samples illustrated an intense peak at about 2.10 ° 2θ assigned to d100 reflection which is the typical sign of hexagonal mesoporous arrangement. The more amounts of zinc, the lower intensity of all reflections, especially in d100 plan can be observed. Consequently, the distinct decrease of structural order is caused by high metal loading and pore fouling. Then, the less intense reflection caused to the more zinc loading. On the other hand, the high angle XRD patterns of zinc incorporated MCM-41 samples (Fig. 3) indicate a peak on 36.0° 2θ assigned to d101 reflection which identifies hexagonal zinc oxide crystals is indeed present inside the pores of the MCM-41.

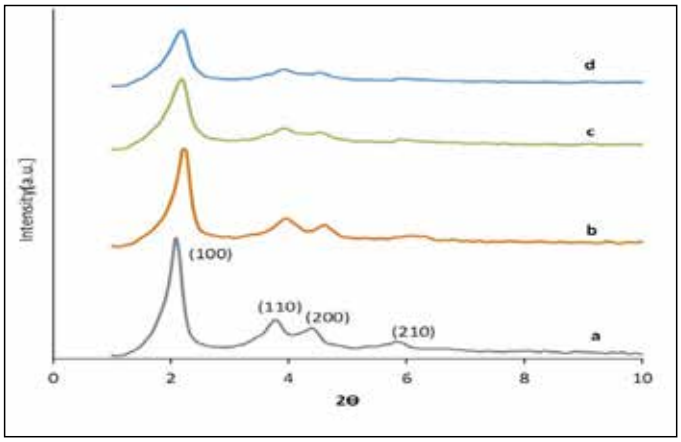

Fig. 2. X-ray diffraction patterns of a) MCM-41 b) Zn3@MCM-41 c) Zn6@MCM-41 d)Zn9@MCM-41

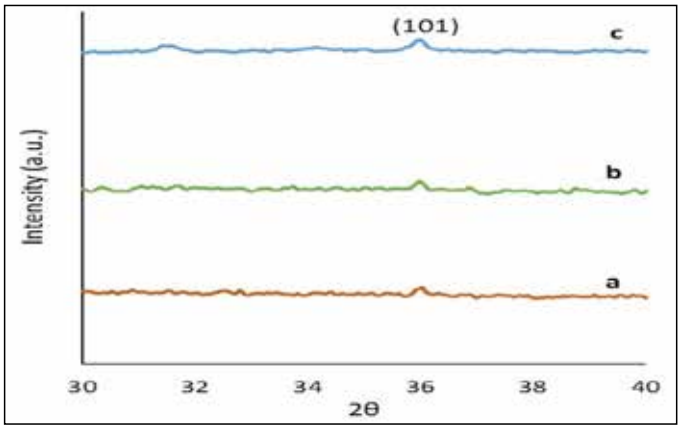

Fig. 3. High angle X-ray diffraction patterns of a) Zn3@MCM-41 b) Zn6@MCM-41 c) Zn9@MCM-41.

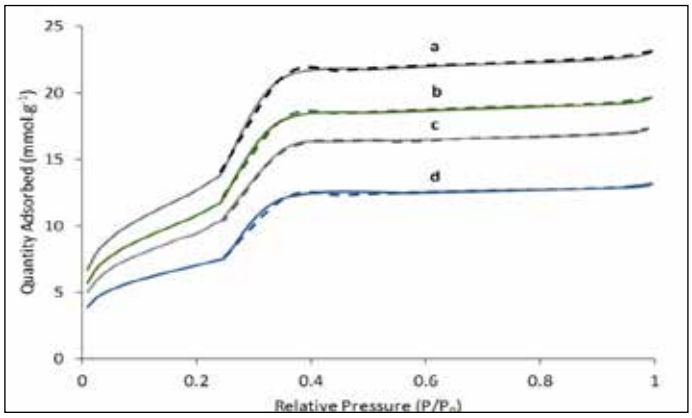

Fig. 4. Nitrogen adsorption isotherms of a) MCM-41 b) Zn3@MCM-41 c) Zn6@MCM-41

Table 1. Textural properties of Znx@MCM-41 zinc-containing samples (x = 0, 3, 6 and 9). a) Volume of mesopores b) d-spacing from XRD (nm) c) Unit cell parameter (nm) d) Pore diameter (nm) e) wall thickness from [a - (Wd/1.050)] equation (nm).

Sample name	S_{BET} (m^2g^{-1})	V_P (cm^3g^{-1})[a]	d (nm)[b]	a (nm)[c]	W_d (nm)[d]	b_d (nm)[e]
MCM-41	1114	0.85	4.01	4.63	3.93	0.89
Zn3@MCM-41	891	0.72	4.24	4.89	4.03	1.06
Zn6@MCM-41	571	0.55	4.05	4.67	3.63	1.21
Zn9@MCM-41	509	0.34	4.12	4.76	3.27	1.65

3.2. N_2 Adsorption.

The well-known, nitrogen physisorption technique was used for determination of the textural properties of prepared porous materials. The N_2 adsorption isotherms of all of the samples are shown in Figure 4. MCM-41 (Fig. 4a) shows a type-IV isotherm, which is a sign to have mesopores. At lower relative pressure (0.2 to 0.3), the adsorption branch of isotherm is expected to be the filling of mesopores stage with liquid nitrogen through capillary condensation. In this stage the sharpness is a sign of size uniformity and structural order of mesopores.

Desorption branch of isotherms accords with the adsorption which is an additional sign of high uniformity of mesopores. Textural properties of Znx@MCM-41 samples obtained from XRD and N_2 adsorption isotherms are tabulated in Table 1. From the table it is observed that the pore volume of the MCM-41 sample is decreased after loading inside the pores and the pores are not completely blocked. Decreasing of specific surface area by more loading indicates insertion of ZnO inside of the mesopores.

3.3. High Resolution TEM (HRTEM)

HRTEM images of Znx@MCM-41 (x=3, 6 and 9) are shown in Figure 5. Based on the obtained results, the high ordered array of the sample shows that the hexagonal structure of mesopores didn't damage in the in-situ loading of zinc.

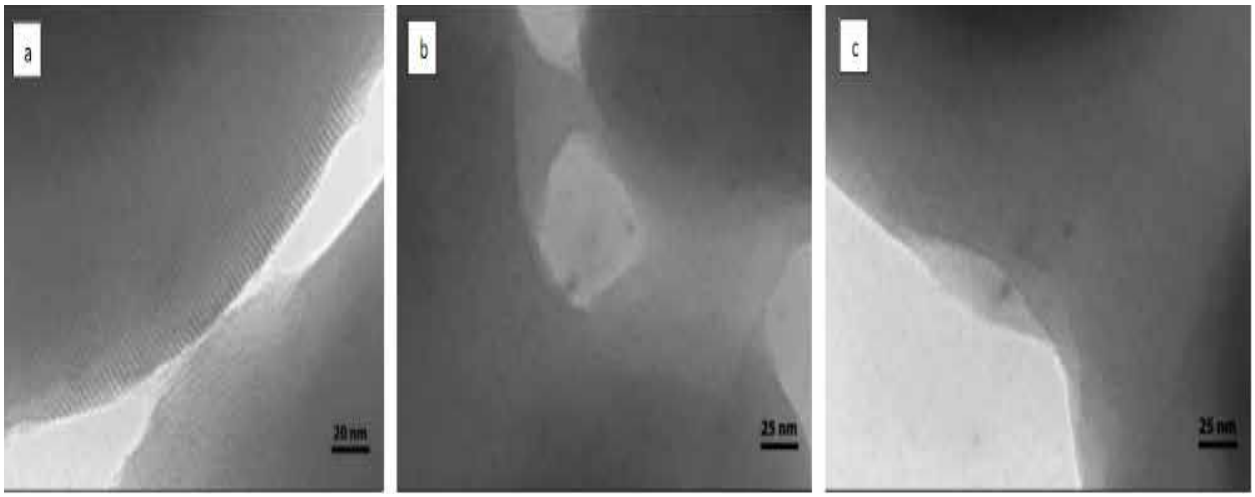

Fig. 5. HR-TEM images of zinc containing MCM-41. a) Zn3@MCM-41 b) Zn6@MCM-41 c) Zn9@MCM-41.

3.4. H_2S Adsorption

Synthesized samples showed great ability to remove H_2S at standard temperatures. As presented in Table 2, the changes of operating conditions were resulted by variation in practical temperature (50, 175 and 300°C), while space velocity in all the experiments was fixed on 3000 h^{-1}. Nine different experiments, designed based on two factors (A: zinc percentage and B: temperature), are shown in Table 2, which also contains the responses in the last column (tbp). The responses define hydrogen sulfide breakpoint in the carrier gas, the minute that H_2S concentration in the outlet gas becomes 5000 ppm.

Table 2. The experimental data of the breakpoints for experiments. (A: Zinc mole percentage B: Temperature tbp: Breakthrough time)

Run	Independent Variables		
	A	B	t_{bp} (min)
Blank	0	50	40.0
1	3	50	135.2
2	3	175	163.1
3	3	300	192.0
4	6	50	171.3
5	6	175	250.2
6	6	300	328.1
7	9	50	232.5
8	9	175	363.4
9	9	300	411.0

3.5. Effect of ZnO content and temperature

In this work, different amounts of zinc oxide were incorporated into the pores of MCM-41 by an in situ approach. It is clear that increasing zinc content at same operating condition (T: 175°C and space velocity: 3000 h^{-1}) caused noticeable increasing of adsorption (Fig. 6). This is attributed to increase in the active sites by rising zinc oxide loading which improves the chemical adsorption of hydrogen sulfide on the materials.

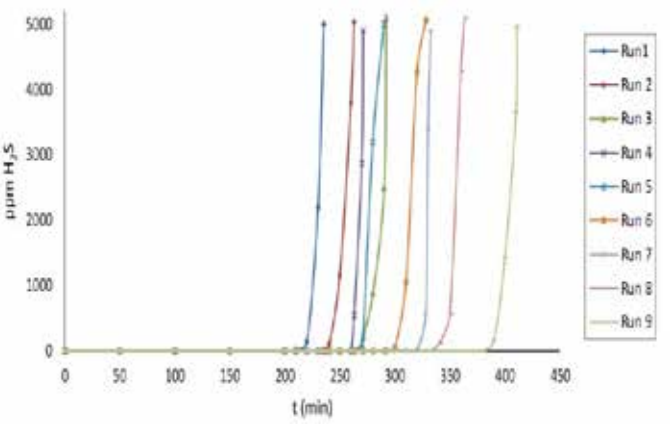

Fig. 6. Breakthrough curves of H_2S adsorption on Znx@MCM-41. The box at the right side of the figure indicates the run number (Table 1).

The effect of temperature was also investigated. With the increase in the temperature of absorption, the H_2S breakthrough was occurred later. Moreover increasing the temperature speeds up the adsorption by strengthening chemisorption of H_2S on ZnO [15], tbp increases as a consequence.

3.6. Effect of metal modification method

The selection of a hydrophobic zinc precursor ($Zn(acac)_2$) is the main reason to lead the zinc particles inside of the mesopores of MCM-41 by the influence of solvent-solute interactions in synthesis process. As comparing to the previous work based on wet impregnation for synthesis of ZnO containing MCM-41 [15], the pore volume and surface area of Zn@MCM-41 by proposed method was higher than previous work. Besides the values of H_2S breakthrough in the same operational condition is considerable. This might be because of the high dispersion and accessibility of zinc nanoparticles inside of the mesopores. Furthermore the smaller size of zinc nanoparticles improves the selectivity and effectiveness of them in the adsorption of H_2S.

3.7. Analysis of variance

The analysis of variance (ANOVA) on tbp is given in Table 3. If the value of F is more than that of the F-table at a similar probability level, the factor or

the interaction is statistically significant. The factors A, B and interaction AB verified to be statistically effective on tbp. The greater F the more significant effects on the response. The level of adsorption is given by regression equation of analysis of variance. It is consist of the linear relationship among all of the effects, and the response of the final equations in terms of effective variables is presented in equation 1:

$$T = +71.14 + 14.43\,A + 0.036\,B + 0.081\,AB \quad \text{(EQ.1)}$$

According to Figure 7, the interaction between two factors may be obtainable which influences on the response (tbp) with the confidence level of 95%. Figure 8 also shows the three-dimensional curves presenting the impact of temperature and zinc percentage on the breakpoints. The slope increase in response, observed on each curve, indicates that the effect of zinc percentage (factor A) on the response is greater than the effect of absorption temperature (factor B).

Table 3. Analysis of variance (ANOVA)

Source	Sum of Square	Degree of freedom	Mean Square	F-value	P-value (Prob>F)	Remark
Model	73838.5	3	24612.8	74.33	<0.0001	significant
A-Zn %	44376.0	1	44376.0	134.01	<0.0001	significant
B-Temp	25741.5	1	25741.5	77.73	0.0003	significant
AB	3721.0	1	3721.0	11.24	0.0203	significant
R-Error	1655.5	5	331.1	-	-	-
C-Total	75494.2	8	-	-	-	-

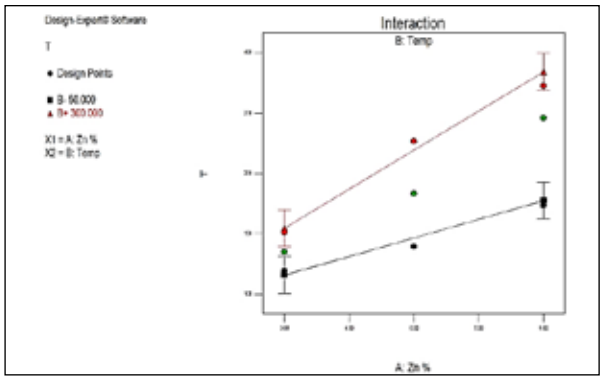

Fig. 7. Interaction between factors and their effect on breakpoint

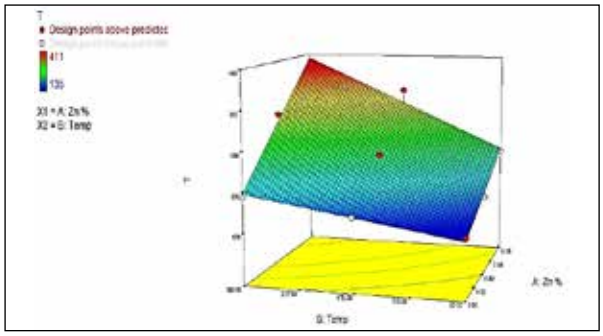

Fig. 8. Three-dimensional curves presenting the impact of factors on response

4. Conclusions

Herein nanoparticles of zinc were successfully immobilized into the mesopores of MCM-41. A significant difference between the presented approach and the typical in-situ pathways is based on the precursor's behavior in the solution. In this process, $Zn(acac)_2$ was located inside the hydrophobic micelles at which they were arranged by surfactant (before adding silica source) and after that, the zinc oxide nanopaticles were anchored onto silica walls. Although the metal precursor was added in the synthesis medium, the introduced metal in silica's walls is less than other in-situ methods. Notably, the characterization techniques showed considerably high specification for all of the samples as mentioned above. The results showed the high capacity of materials to adsorb H_2S. H_2S removal from LPG cut of the studied crude oil in the point of Zn= 9 wt. % and T = 300°C was adsorbed for about 7 hours in space velocity of 3000 h^{-1}. Additionally, the comparison between this work with the other published method showed, the more ability and efficienty extraction of H_2S gas.

5. Acknowledgements

The authors wish to thank from Amirkabir University of Technology, Tehran, Iran, Iranian Research Institute of Petroleum Industry (RIPI) for supporting of this work.

6. References

[1] C. Bensing, M. Mojić, S. Gómez-Ruiz, S. Carralero, B. Dojčinović, D. Maksimović-Ivanić, S. Mijatović, G.N. Kaluderović, Evaluation of functionalized mesoporous silica SBA-15 as a carrier system for Ph3Sn(CH2)3OH against the A2780 ovarian carcinoma cell line, Dalton Trans., 45 (2016) 18984-18993.

[2] Y. Wan, D. Zhao, On teh controllable soft-templating approach to mesoporous silicates, Chem. Rev., 107 (2007) 2821–2860.

[3] A. Sterczynska, A. Derylo-Marczewska, M. Zienkiewicz-Strzalka, M. Sliwinska-Bartkowiak, K. Domin, Surface properties of Al-functionalized mesoporous MCM-41 and teh melting behavior of water in Al-MCM-41 nanopores, Langmuir, 33 (2017) 11203–11216.

[4] F.J. Carmona, I. Jimenez-Amezcua, S. Rojas, C.C. Romao, J.A. Navarro, C.R. Maldonado, E. Barea, Aluminum doped MCM-41 nanoparticles as platforms for the dual encapsulation of a CO-releasing molecule and cisplatin, Inorg. Chem., 56 (2017) 10474-10480.

[5] M. Abdouss, N. Hazrati, A.A. Miran-Beigi, A. Vahid, A. Mohammadalizadeh, Effect of the structure of the support and the aminosilane type on the adsorption of H_2S from model gas, RSC Adv., 4 (2014) 6337-6345.

[6] M. Thommes, K. Kaneko, A.V. Neimark, J.P. Olivier, F. Rodriguez-Reinoso, J. Rouquerol, K.S. Sing, Physisorption of gases, with special reference to the evaluation of surface area and pore size distribution (IUPAC Technical Report), Pure Appl. Chem., 87 (2015) 1051-1069.

[7] V.B. Cashin, D.S. Eldridge, A. Yu, D. Zhao, Surface functionalization and manipulation of mesoporous silica adsorbents for improved removal of pollutants: a review, Environ. Sci. Water Res. Technol., 4 (2018) 110-118.

[8] E. Dündar-Tekkaya, Y. Yürüm, Int. J. Hydrog, Mesoporous MCM-41 material for hydrogen storage: A short review, Int. J. Hydrog. Energ., 41 (2016) 9789-9795.

[9] E. Lovell, Y. Jiang, J. Scott, F. Wang, Y. Suhardja, M. Chen, J. Huang, R. Amal, CO2 reforming of methane over MCM-41-supported nickel catalysts: altering support acidity by one-pot synthesis at room temperature, App. Catal. A: General, 473 (2014) 51-58.

[10] B.S. Kim, C.S. Jeong, J. M. Kim, S.B. Park, S.H. Park, J.K. Jeon, S.C. Jung, S.C. Kim, Y.K. Ex Situ, Catalytic upgrading of lignocellulosic biomass components over vanadium contained H-MCM-41 catalysts, Catal. Today, 265 (2016) 184-191.

[11] M. Fadhli, I. Khedher, J.M. Fraile, J. Mol. Catal, Modified Ti/MCM-41 catalysts for enantioselective epoxidation of styrene, J. Mol.

Catal. A Chem., 420 (2016) 282-289.

[12] WY. Sang, OP. Ching, Tailoring MCM-41 mesoporous silica particles through modified sol-gel process for gas separation, AIP Conf. Proc., 1891 (2017) 020147.

[13] E. Beňová, V. Zeleňák, D. Halamová, M. Almáši, V. Petrul'ová, M. Psotka, A. Zeleňáková, M. Bačkor, V. Hornebecq, A drug delivery system based on switchable photo-controlled p-coumaric acid derivatives anchored on mesoporous silica, J. Mater. Chem. B, 5 (2017) 817-825.

[14] JJ. Zhang, WY. Wang, GJ. Wang, C. Kai, H. Song, L. Wang, Equilibrium, kinetic and thermodynamic studies on adsorptive removal of H_2S from natural gas by amine functionalisation of MCM-41. Prog. React. Kinet. Mec., 42 (2017) 221-234.

[15] N. Hazrati, M. Abdouss, A. Vahid, A. A. Miran Beigi, A. Mohammadalizadeh, Removal of H 2 S from crude oil via stripping followed by adsorption using ZnO/MCM-41 and optimization of parameters, Environ. Sci. Technol., (2014) 997-1006.

[16] Y.S. Hong, Z.F. Zhang, Z.P. Cai, X.H. Zhao,B.S. Liu, Deactivation kinetics model of H_2S removal over mesoporous LaFeO3/MCM-41 sorbent during hot coal gas desulfurization. Sustain, Energ. Fuels, 28 (2014) 6012-6018.

[17] X. Feng, Z. Yan, N. Chen, Y. Zhang, X. Liu, Y. Ma, X. Yang, W. Hou, Synthesis of a graphene/ polyaniline/MCM-41 nanocomposite and its application as a supercapacitor. New J. Chem., 37 (2013) 2203-2209.

[18] Y. Bao, X. Yan, W. Du, X. Xie, X. Pan, J. Zhou, L. Li, Application of amine-functionalized MCM-41 modified ultrafiltration membrane to remove chromium (VI) and copper (II), Chem. Eng. J., 281 (2015) 460-4607.

[19] D.P. Sahoo, D. Rath, B. Nanda, K. Parida, Transition metal/metal oxide modified MCM-41 for pollutant degradation and hydrogen energy production: a review, RSC Adv., 5(2015) 83707-83724.

[20] E.P. Baston, A.B. Franca, A.V. da Silva Neto, E.A. Urquieta-Gonzalez, Incorporation of the precursors of Mo and Ni oxides directly into the reaction mixture of sol–gel prepared γ-Al2O3-ZrO2 supports evaluation of the sulfided catalysts in the thiophene hydrodesulfurization, Catal. Today, 246 (2015) 184-190.

[21] A. Kowalczyk, A. Borcuch, M. Michalik, M. Rutkowska, B. Gil, Z. Sojka, P. Indyka, L. Chmielarz, MCM-41 modified with transition metals by template ion-exchange method as catalysts for selective catalytic oxidation of ammonia to dinitrogen, Micropor. Mesopor. Mater., 240 (2017) 9-21.

[22] KS. Kamarudin, NO. Alias, Adsorption performance of MCM-41 impregnated with amine for CO2 removal, Fuel Process. Technol., 106 (2013) 332-337.

[23] S. Qiu, X. Zhang, Q. Liu, T. Wang, Q. Zhang, L. Ma, A simple method to prepare highly active and dispersed Ni/MCM-41 catalysts by co-impregnation, Catal. Commun., 42 (2013) 73-78.

[24] R. Atchudan, S. Perumal, TN. Edison, YR. Lee, Highly graphitic carbon nanosheets synthesized over tailored mesoporous molecular sieves using acetylene by chemical vapor deposition method, RSC adv., 5 (2015) 93364-93373.

[25] AA. Gewirth, JA. Varnell, AM. Di Ascro. Nonprecious metal catalysts for oxygen reduction in heterogeneous aqueous systems, Chem. Rev., 118 (2018) 2313-2339.

[26] B. Elyassi, Y. Al Wahedi, N. Rajabbeigi, P. Kumar, J.S. Jeong, X. Zhang, P. Kumar, V.V. Balasubramanian, M.S. Katsiotis, K.A. Mkhoyan, N. Boukos. A high-performance adsorbent for hydrogen sulfide removal, Micropor. Mesopor. Mater., 190 (2014) 152-155.

[27] S. Jafarinejad, Control and treatment of sulfur compounds specially sulfur oxides (SOx) emissions from the petroleum industry: a review, Chem. Int., 2 (2016) 242-253.

[28] P.R. Westmoreland, D.P. Harrison, Evaluation of candidate solids for high-temperature desulfurization of low-Btu gases, Environ. Sci. Technol., 10 (1976) 659-661.